Development of orientation during electrospinning of fibres of poly(ε-caprolactone)

Article

Accepted Version

Development of orientation during electrospinning of fibres of poly(ε-caprolactone)

Matthew D Edwards, Geoffrey R Mitchell*, Saeed D Mohan and Robert H Olley

Polymer Science Centre, University of Reading, Reading RG6 6AF UK

Email: g.r.mitchell@reading.ac.uk

FAX + 44 118 9750203

12 December 2009

Submitted to the European Polymer Journal

Keywords: electrospinning; orientation; crystallisation; poly(ε-caprolactone); x-ray scattering

Abstract

We explore the influence of a rotating collector on the internal structure of poly (ε-caprolactone) fibres electrospun from a solution in dichloroethane. We find that above a threshold collector speed, the mean fibre diameter reduces as the speed increases and the fibres are further extended. Small-angle and wide-angle X-ray scattering techniques show a preferred orientation of the lamellar crystals normal to the fibre axis which increases with collector speed to a maximum and then reduces. We have separated out the processes of fibre alignment on the collector and the orientation of crystals within the fibres. There are several stages to this behaviour which correspond to the situations (a) where the collector speed is slower than the fibre spinning rate, (b) the fibre is mechanically extended by the rotating collector and (c) where the deformation leads to fibre fracture. The mechanical deformation leads to a development of preferred orientation with extension which is similar to the prediction of the pseudo-affine deformation model and suggests that the deformation takes place during the spinning process after the crystals have formed.

1. Introduction

Electrospinning generates nano and micro-scale polymer fibres by means of applying an electric field to droplets of polymer solution passed from tip of a fine orifice [1]. As a consequence of Coulombic forces, a droplet of the solution of a polymer will become charged; as a consequence its shape will become distorted to form a cone-like geometry [2]. Dependent on the strength of the electric field together with the viscosity, surface tension and dielectric properties of the solution, the integrity of the droplet will break down and a fibre of polymer will be produced and deposited on the collector. Initally, the droplet produces a jet which extends away from electrode in more or less a straightline, but then it is bent in to a complex path during which the electric forces extend the fibre, substantially reducing the diameter of the fibre [3,4].. As a consequence of the jet instabilities, the fibres form a random mat on the electrode and there is a random orientation of the fibres with in the plane of the electrode. .Recent interest in this technique arises not only from the topicality of nanoscale material fabrication, but also from the potential use of these fibres in a range of applications which include filtration, drug delivery and the use of scaffolds to provide a framework for tissue regeneration in both soft and hard tissue systems [5].

Poly(ε-caprolactone), referred to here as PCL, has attracted attention as a biomaterial in the tissue scaffolding applications area largely because it is non-toxic, has a slow degradation rate, and the products of biodegradation are also non-toxic [6]. In addition, the material is highly elastic compared to other non toxic polyesters and has interesting mechanical properties combining both crystallisation and rubbery behaviour, compatible with, for example, vascular applications. The tensile strengths of electrospun fibres tend to be rather low compared to thicker fibres produced using

conventional drawing techniques. Clearly, the control of structure and the semi-crystalline morphology of the fibre material are critical to the process of improving the mechanical properties. A number of reports have highlighted the potential of a rotating collector to align fibres along a common axis including work on PCL [7], polyacrylonitrile [8], polyoxymethylene [9] and nylon-6 [10]. Here we explore how the level of preferred orientation within the nanoscale fibres and the alignment of the fibres on the collector are affected by the electrospinning process using a rotating collector electrode.

2. Experimental Part

2.1. Materials

The polymer used throughout this work was poly(ε-caprolactone) with Mw = 80,000 Da supplied by Aldrich. Solutions of 30% w/v PCL in dichloroethane were prepared at room temperature (20-25°C).

2.2. Electrospinning

Electrospinning was performed using the system shown schematically in Figure 1. The system consisted of a glass syringe mounted in a syringe pump fitted with a 17 gauge needle of length 6 cm and with an internal diameter of 1.1 mm together with a rotating drum electrode placed 25 cm from the needle. The drum had an external diameter of 3.2 cm and a length of 9.2 cm. The drum was coated with an aluminium foil which was earthed. The tangential velocity of the rotating electrode could be varied from 0 to 8m/s. A Glassman High Voltage power supply was used which allowed defined voltages over the range 7.5 - 20 kV. During the preparation of the electrospun fibres the temperature was 19 ± 1°C and the relative humidity was 37 ± 5%.

2.3. X-ray scattering

Wide-angle X-ray scattering (WAXS) data were obtained for processed samples at room temperature over an extended $|\underline{Q}|$ range using a symmetrical transmission diffractometer equipped with a graphite monochromator and pinhole collimation and a Cu K X-ray source. Data for anisotropic samples were obtained both as a function of $|\underline{Q}|$ over the range 0.2 to 6 $Å^{-1}$ in steps of 0.02 $Å^{-1}$ and of α over the range 0° to 90°

in steps of 5°, where α is the angle between the symmetry axis of the sample and the scattering vector Q and $|\underline{Q}| = 4\pi\sin\theta/\lambda$, where λ is the incident wavelength and 2θ is the scattering angle.

Small-angle X-ray scattering (SAXS) experiments were performed on the fixed wavelength (λ=1.54 Å) A2 Beam Line at DESY Hamburg using a beam ~ 0.3 mm diameter. Data were recorded using a 2-D MAR CCD detector in a symmetrical arrangement mounted ~3m from the sample using an extended vacuum tube. This allowed scattering data to be accumulated in the range $|\underline{Q}|$ ~ 0.005 to 0.1 $Å^{-1}$. The scattering geometry was calibrated using a dry collagen fibre. Some WAXS data were obtained using a similar arrangement but with a sample to detector distance of ~0.1m and without the vacuum tube.

2.4. Microscopy

Scanning electron microscopy was performed using a FEI Quanta 600 SEM equipped with a field emission gun. The fibres were coated with gold prior to examination.

3. Results

Electrospun fibres were easily prepared using a voltage of 10kV. Figures 2a and 2b compare the scanning electron microscope images of fibres collected on a static electrode with those collected on a rotating electrode with a tangential velocity of 4.3m/s. It is clear that the sample prepared with the rotating collector exhibits a very high level of common alignment of the fibres parallel to the tangential velocity vector. In each case the fibres are smooth, free from beading and exhibit a close to circular cross-section. Scanning electron micrographs were used to evaluate the fibre diameter distribution using measurements taken from across the material; sampling was performed using a grid to reduce any subjectivity therein. Figure 2c shows the distribution of fibre diameters for the material prepared with a collector speed of 4.3m/s. This sample exhibits a monomodal distribution with a mean of ~ 7μm and a width at half height of ~ 2μm.

A systematic series of fibres were prepared under the same conditions as described above for a range of rotation speeds for the collector. At all collector speeds, fibres were easily prepared. At the highest speeds (i.e. > 6m/s) the yield of fibres on the collector was slightly smaller. As we will discuss later, the higher collector speeds lead to an increase in the breakage of the fibres and as a consequence, some were not collected on the electrode. . Subsequent scanning electron microscopy showed that the diameter of the electrospun fibres varied with the collector speed used in their preparation. Figure 3 shows the variation of the fibre diameter with the tangential velocity of the collector drum for a sample of ~ 100 fibres. The bars in Figure 3 represent the width of the fibre diameter distribution at half height (FWHM). Interestingly, there appears to be a small increase in the mean fibre diameter with

increasing collector rotation speed at low speeds, but for speeds > 2m/s there is a steady reduction in the fibre diameter. We have noted that in other material systems studied in our laboratory and elsewhere a small increase in the fibre diameter with increasing collector speed was observed [7,11].

If we take the density of the fibres to be constant and independent of the rotation speed used in their preparation, we can utilise the fibre diameter data to estimate an effective extension ratio, λ, for the fibres as compared to those prepared with a static collector. Consider two fibre samples with the same mass but fibre diameters d_1 and d_2, contour lengths l_1 and l_2 and densities $\rho_1=\rho_2$:

$$\frac{\rho_1 l_1 \pi d_1^2}{4} = \frac{\rho_2 l_2 \pi d_2^2}{4} \qquad (1)$$

$$\lambda = \frac{l_2}{l_1} = \frac{d_1^2}{d_2^2} \qquad (2)$$

The estimate of the extension ratio, λ, for each sample is plotted against the collector tangential speed in Figure 3. The data exhibit two clear phases of behaviour. At very low collector speeds there is a little variation in the fibre diameter whilst for speeds greater than 2m/s there is a continual increase in the effective fibre extension ratio with rotator speed, reaching, reach an extension ratio of ~ 10 at a collector speed of 7m/s. In this second phase it is clear that the fibres have been deformed by the process of collection on to the rotating drum electrode.

Examination of the orientation of individual fibres on the surface of the rotating collector shows that there is a progression from the expected random arrangement when the collector is static to a high level of common alignment of the fibres when the collector is rotating. We have measured the angle, β, between an individual fibre

segment and the direction of rotation of the collector. We have evaluated the distribution of the values of β for each sample of fibres corresponding to the range of tangential velocities considered. The orientation distributions, f(β) found for each set of fibres are shown in Figure 4. We have used these data to calculate the first three orientation parameters, $\langle P_2 \rangle_f$, $\langle P_4 \rangle_f$, $\langle P_6 \rangle_f$ which describe the orientation distribution functions f(β) for each set of fibres [12,13,14]. For parallel alignment of the fibres with respect to the rotation axis, $\langle P_2 \rangle_f$, $\langle P_4 \rangle_f$, $\langle P_6 \rangle_f$ will be equal to 1 and for a random orientation these parameters will have a value equal to 0. The values of these orientation parameters for each set of fibres are plotted in Figure 5 as a function of the tangential velocity of the rotating collector. These orientation parameters increase with increasing velocity with a peak value at a velocity ~ 2.5 m/s. The values of all three orientation parameters increase towards 1, reflecting a narrowing of the orientation distribution as may be seen in Figure 4. At higher velocities there is a small drop in the level of preferred orientation which then increases further with additional increase in the tangential velocity. The orientation distribution functions for the fibres prepared at higher velocities show a maximum at an angle which shifts slightly away from β=0°.

We have superimposed a plot of the mean diameter of the fibres on Figure 5. This shows that at the point of the maximum of the fibre orientation at a velocity of ~ 2.5m/s, the fibre diameter has already reduced from the value recorded for the static collector. In other words, the fibre being wound on to the collector is both under tension and has been drawn down. This confirms the expected behaviour that the fibre winding process is affected by the tension and it is the tension which allows a near parallel alignment of the fibres.

Fibres taken from the rotating collector were examined using small-angle and wide-angle X-ray scattering procedures. The scattering patterns are obtained from bundles of fibres held in the same macroscopic alignment as taken from the collector electrode. In all cases, the rotation direction is vertical on the page. Figure 6 shows the WAXS and SAXS patterns for fibres prepared at four different collector speeds. The wide-angle scattering patterns show that all the fibres exhibit a semi-crystalline structure. The prominent crystalline peaks correspond to the (110) and (200) peaks for the crystal structure of PCL [15]. The WAXS pattern obtained from the sample for a collector speed of 0.8m/s shows an almost constant intensity value around each ring indicative of a largely isotropic distribution of crystals or more precisely the (110) and (200) crystal planes. The pattern obtained for the sample prepared with a collector speed of 2.5m/s shows strong arcing on the crystal peaks indicating a substantial level of preferred orientation. This is more marked at higher collector speeds.

The SAXS patterns show the same increase in preferred orientation with increasing collector speed. The SAXS pattern is typical for a semi-crystalline polymer and shows intense scattering in the form of peaks above and below the zero-angle position which arise from the thin lamellar crystals which generally form in polymers. The peak position gives a long period of 160Å which is a little smaller than the value typical for melt crystallised PCL of 180Å [16]. The anisotropic scattering around the beam stop probably arises from voids in the fibre sample [17]. The increase in the level of preferred orientation of the lamellar crystals indicated in the WAXS patterns is shown clearly in the SAXS patterns. The level of preferred orientation can qualitatively be judged by the width of the azimuthal arcing of the peaks. On this basis the level of lamellar orientation is greatest in the pattern obtained from the sample prepared with a collector speed of 4.3m/s.

To enable a quantitative measure of the level of preferred orientation of the lamellar crystals we have utilised a 3-circle X-ray diffractometer to obtain high quality WAXS intensity data over a complete quadrant of reciprocal space. The data for the sample prepared with a collector speed of 4.3m/s are shown in Figure 7 along with azimuthal variation of intensity for the (110) peak. We have utilised this azimuthal variation in intensity recorded for each sample to calculate the level of preferred orientation $\langle P_2 \rangle$ of the (110) crystal planes with respect to the overall sample axis using methodologies described in detail elsewhere [12,13].

The results are shown in Figure 8 plotted against the extension ratio evaluated as described previously. If the level of preferred orientation is zero $\langle P_2 \rangle = 0.0$, and $\langle P_2 \rangle = 1$ corresponds to the situation where there is a single orientation of the crystal planes. At low extension ratios there are modest level of preferred orientation but the extent of orientation increases with increasing values of the extension ratio and it reaches a maximum for an extension ratio ~ 5. At higher extension ratios the level of preferred orientation is still significant but considerably less than the maximum.

The level of preferred orientation measured in these experiments is an average over a number of fibres. If there is a variation in the spread of alignment of the fibres within the sample this will affect the level of the preferred orientation observed by X-ray scattering. In fact, the orientation distribution of the crystals in the complete sample, $f_x(\gamma)$ is the convolution of the fibre axis orientation distribution $f_f(\beta)$ and the orientation distribution of the crystals with respect to the axis of the fibre $f_c(\chi)$ as in [14,18]:

$$f_x = f_c * f_f \quad (3)$$

Figure 9 shows schematically the geometry, the reference axes and the angles. We have measured the macroscopic alignment of fibres, $\langle P_2 \rangle_f$, $\langle P_4 \rangle_f$, $\langle P_6 \rangle_f$, within each sample as shown in Figures 4 & 5. A particular advantage of describing the levels of preferred orientation using the series of spherical harmonics $\langle P_2 \rangle$, $\langle P_4 \rangle$, $\langle P_6 \rangle$ etc. is that we can write the convolution in equation 3 using the Legendre addition theorem as [14,18]:

$$\langle P_2 \rangle_x = \langle P_2 \rangle_c \langle P_2 \rangle_f \quad (4)$$

where $\langle P_2 \rangle_x$ is the orientation of the crystal planes measured by X-ray scattering with respect to the rotation direction of the collector, $\langle P_2 \rangle_f$ is the orientation parameter describing the fibre alignment on the collector with respect to the rotation direction and $\langle P_2 \rangle_c$ describes the orientation of the crystals within a fibre, in other words with respect to the fibre axis. We can write similar expressions to that in Equation 4 for higher order orientation parameters such as $\langle P_4 \rangle$, $\langle P_6 \rangle$ etc.

As a consequence that we can evaluate the level of crystal alignment within an average fibre, thereby eliminating the effect of the distribution of fibre alignments on the rotating collector using:

$$\langle P_2 \rangle_c = \frac{\langle P_2 \rangle_x}{\langle P_2 \rangle_f} \quad (5)$$

We have used equation 5 to calculate the orientation of the crystal orientation with an average fibre i.e. $\langle P_2 \rangle_c$ and these results are plotted in Figure 10 as a function of the extension ratio calculated in Figure 3.

In Figure 10 we have also compared the measured levels of preferred orientation of the crystals in a fibre with those predicted by the pseudo-affine model for deformation

[19]. There is broad similarity in the rate of development of orientation with extension ratio up to ~ 5.

4. Discussion

The use of a rotating collector leads to the formation of aligned arrays of PCL fibres on the collector. We have shown how the fibre diameter, the fibre alignment and the alignment of crystals which form within the fibres vary with the tangential velocity of the collector. It is convenient to consider the variation in behaviour of these macroscopic and microscopic parameters with increasing collector rotation speed in a number of stages.

The first stage corresponds to tangential velocities of less than 2m/s and in this region the 'windup' speed is less than the jet velocity. We deduce this from the observation that there is no draw down of the electrospun fibres (Figure 3). In other words the fibres are not under a significant mechanical tension. Fibres which are collected by the rotator will lie at a variety of angles. For tangential velocities greater than 2m/s (stage 2) the fibre diameter reduces with increasing collector speed and hence this places each fibre under a mechanical tension. This favours the so-called hoop alignment of fibres on to the rotating cylinder such that they lie parallel to the rotation direction. This type of behaviour has been widely observed and modelled in connection with the technology of filament winding, for example [20,21]. As a consequence of the tension in the fibre, the fibres wind-up on the collector with an orientation distribution centred on $\beta=0°$. We find that the peak in the orientation distribution of the fibres on the collector occurs at a tangential velocity within this draw down stage, namely 2.5m/s. Wu et al [7] proposed that such an arrangement would occur when the tangential velocity and the jet velocity are equal. For a PCL/dichloromethane/methanol system they observed a maximum fibre orientation at a tangential velocity of 2m/s and interestingly they also observed fibres prepared at a

low collector speed which were thicker than those produced with a static collector as observed in this study.

We have used WAXS and SAXS to probe the internal structure of the PCL fibres. We find that each set of fibres exhibits a semi-crystalline structure in which the major variation is the level of preferred orientation; other structural parameters such as crystal structure, crystallinity or long period are essentially constant. The data presented in Figure 10 has been corrected for the distribution of the alignment of fibres within the sample and so the data represents the crystal orientation with respect to the fibre axis. It is clear that the crystal orientation reaches a maximum at an extension ratio of 5 or a collector velocity of ~ 5m/s and then drops away as the collector rotation speed increases further. We attribute this to breakage of the fibres as the mechanical tension rises with increasing collector speed. The work of Williamson and Coombes [22] showed that gravity spun fibres of PCL prepared from solution exhibited extension at break values ranging from 1.75 to 6.08 dependent on the processing conditions. The estimate of the typical breakage observed here is towards the upper end of this range. Fennessey et al [8] showed that the level of orientation in polyacrylonitrile electrospun fibres increased continuously with rotating collector speed until it reached a plateau at a tangential velocity of 9.8m/s. Even higher collector velocities up to 31.5m/s. were explored in a study of polyoxymethylene system [9], while similar studies with nylon-6 revealed that the level of orientation reached a plateau of 5m/s which was then maintained up to 15m/s [10]. These reports and the work of Wu et al [7] lend support to the proposal above that the drop in the level of preferred orientation for velocities greater than 5m/s is due to fibre breakage.

PCL is a semi-crystalline polymer and it is well established that the environment present prior to and during the early stages of crystallisation is crucial to templating or directing the crystallisation process. The formation of crystals during electrospinning of PCL solutions will involve the loss of solvent as well as the crystallisation of the polymer itself. If the conformations of some polymer chains are extended during the electrospinning process these may act as row nuclei for the subsequent crystallisation of the remaining polymer. In such a situation, the level of preferred orientation of the crystals will depend on the fraction of row nucleated crystals and those which have formed from randomly oriented nuclei. In the case of uniaxially extended rubber systems [23] or in polymers crystallised from sheared melts [24,25] the row nuclei are more or less perfectly aligned with respect to the external flow or stress field. If crystals form at an early point of the fibre formation, subsequent extension of the fibre may lead to rotation of the crystals and the development of a significant level of preferred orientation. The most appropriate model for such systems is the pseudo-affine deformation model [19,26] in which the crystals rotate affinely with respect to the surrounding deforming matrix but do not change shape. Figure 10 shows that the prediction of the pseudo-affine model for uniaxial extension compares to a reasonable extent to the observed orientation up to the point where the fibres start to fracture. A more detailed model would need to account for any solvent present at the point of deformation. Such a modification might account for the apparent small offset in the extension ratio values between the model and the observed data.

The generation of an aligned array of electrospun fibres is both critical to some end-use applications and enables the study of those properties in terms of anisotropic properties and structure. This work shows that the velocity of the collector needs careful selection to ensure that the electrospun fibres obtained are representative of

the electrospinning rather than any subsequent deformation stages. In our own work this has proved crucial in the study of polymer conformations of electrospun fibres using small-angle neutron scattering techniques [11].

5. Conclusions

We have shown that, for the poly(ε-caprolactone)/dichloroethane system considered here with a rotating collector, the internal and external structure development takes place in a number of distinct phases namely:

(a) When the collector speed is slower than the fibre spinning rate, the fibres are not deformed and there is partial alignment of the fibres on to the collector;

(b) At higher collector speeds the fibre is mechanically extended by the rotating collector and the ensuing tension leads to the generation of fibres highly aligned on the collector;

(c)At even higher collector speeds, the deformation of the fibre leads to a high level of preferred orientation of the crystals within the fibres which maps on to a model of pseudo-affine deformation suggesting that the crystals form prior to the drawing process;

(d) Ultimately, the deformation of the fibres leads to fracture and the level of crystal orientation drops. Observation of this stage depends on the mechanical properties of the fibres.

These studies show that the optimisation of the rotating collector speed enables control of the external and internal structure of electrospun fibres and hence definition of properties for specific applications. Where aligned arrays of fibres are produced for structural analysis, careful selection of the rotation speed is required to ensure that the fibres are representative of the electrospinning process rather than any subsequent mechanical drawing.

6. Acknowledgements

The scanning electron microscope images were taken using the facilities of the Centre for Advanced Microscopy at Reading. We thank Dr Sérgio Funari for his assistance with the X-ray scattering measurements on the A2 beam-line at the Deutsches Elektronen-Synchrotron (DESY) supported by the European Community (RII3-CT-2004-506008 (IA-SFS).

7. References

1. Greiner A, Wendorff JH. Angew. Chem. Int. Ed., 2007; 46; 5670 – 5703

2. Taylor GI. Proc. R. Soc. Lond. A 1964; 280(1382): 383-397

3. Reneker DH, Yarin AL, Fong H and Koombhongse S J. Appl. Phys. 2000 87, 4531

4. Sin YM, Hohman MM, Brenner MP and Rutledge GC Polymer 2001 42 9955-9967

5. Lannutti J, Reneker D, Ma T, Tomasko D,Farson D. Materials Science and Engineering: C, 2007; 27: 504-509

6. Gaumer J, Prasad A,Lee D, Lannutti J Acta Biomaterialia, 2009; 5: 1552-1561

7. Wu Y, Carnell LA, Clark RL. Polymer 2007; 48: 5653-5661

8. Fennessey SF, Farris RJ Polymer 2004; 45: 4217–4225

9. Kongkhlang T, Tashiro K, Kotaki M, Chirachanchai S, J. Am. Chem. Soc., 2008; 130: 15460–15466

10. Lee K-H, Kim K-W, Pesapane A, Kim H-Y, Rabolt JF *Macromolecules* **2008**; **41**: *1494*-1498

11 Mohan SD, Davis FJ, Olley RH, Sen S, Mitchell GR. submitted to Soft Matter

12 Mitchell GR, Windle AH. Orientation in Liquid Crystal Polymers in Developments in Crystalline Polymers 2 Ed. D.C.Bassett Applied Science 1988. 115-175

13 Mitchell GR, Saengsuwan S,Bualek-Limcharoen S. Progress in Colloid and Polymer Science 2005; 130: 149-159

14. Mitchell GR. J Phys: Conference Series in press 2010

15 Chatani Y, Okita Y, H.Tadokoro H, Yamashita Y. Polymer J 1970; 1: 555-562.

16. Wangsoub S, Olley RH, Mitchell GR. Macromol Chem Phys 2005; 206 :1826-1839

17. Murthy NS. "Structure Formation in Polymeric Fibres" D.R. Salem, Editor. Carl Hanser Verlag: Munich. 2001. p. 475-491.

18. Lovell R, Mitchell GR. Acta Cryst 1981; A37: 135-137

19. Bower DI. An Introduction to Polymer Physics Cambridge University Press 2002. p326

20. Koussios S, Bergsma OK, Beukers A. Composites 2004; A35: 181-195

21. Koussios S, Bergsma OK, Beukers A. Composites 2004; A35: 197-212

22. Williamson MR, Coombes AGS. Biomaterials 2004; 25: 459-465

23. Mitchell GR. Polymer 1984; 25: 1562-1572

24 Pople JA, Mitchell GR, Sutton SJ, Vaughan AS, Chai C. Polymer 1999; 40 2769-2777

25. Keller A, Kolnaar HWH. "Processing of Polymers" Meijer HEH ed. 1997. 18: 189-268

26. Ward IM, "Structure and properties of oriented polymers", Applied Science Publishers, London 1975.

8. Figure Captions

1. Schematic of the electrospinning system with a rotating collector used in this work.

2. Scanning electron microscope micrograph of PCL fibres prepared with (a) static collector and (b) rotating collector with a tangential velocity of 4.3m/s. (c) fibre diameter distribution for the sample prepared with a tangential velocity of 4.3m/s.

3. A plot of the mean fibre diameter (solid circles) against the tangential velocity of the rotating collector (the vertical bars represent the width of the diameter distribution) and a plot of the extension ratio derived from the diameter data.

4. Orientation distribution functions $f_f(\beta)$for the electrospun fibres prepared using the indicated tangential velocities

5. Orientation parameters for the fibre distributions calculated from the data shown in Figure 4 superimposed on a plot of the mean fibre diameter.

6. Wide-angle X-ray scattering patterns (top) for electrospun fibres of PCL prepared using the indicating tangential velocities and the small-angle X-ray scattering patterns for the same samples. The outer edge of the SAXS patterns corresponds to $|\underline{Q}| = 0.08 Å^{-1}$.

7. (a) Wide-angle X-ray scattering function $I(|\underline{Q}|, \alpha)$ for a sample of PCL electrospun fibres prepared with a tangential velocity of 4.3m/s (b) The intensity function $I(\alpha)$ for $|\underline{Q}| = 1.48 Å^{-1}$

8. Plot of the $\langle P_2 \rangle_x$ describing the orientation of the PCL crystals with respect to the rotation direction as a function of the collector tangential velocity used to prepare the samples.

9. Definition of the angles used to describe the orientation of the fibres and the crystals with the fibres.

10. Plot of the $\langle P_2 \rangle_c$ describing the orientation of the PCL crystals with respect to the fibre axis as a function of the collector tangential velocity used to prepare the samples. The solid line corresponds to the pseudo-affine deformation model. The open circles correspond to the samples in which significant fibre breakage has taken place.

Figures

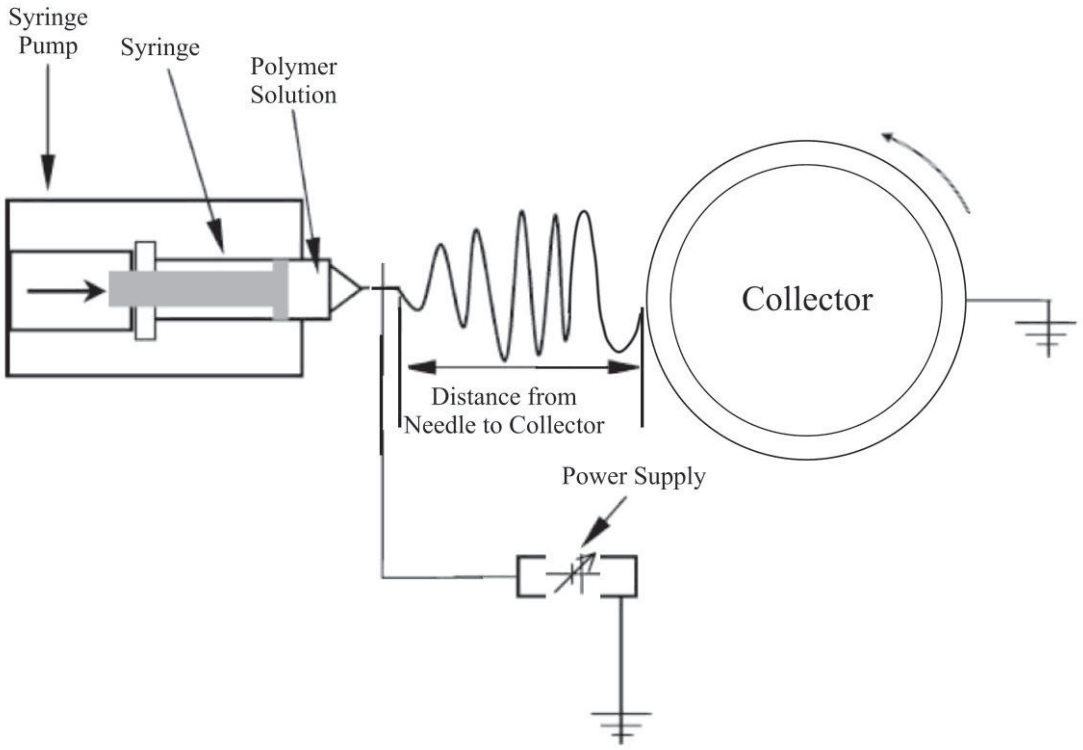

Figure 1

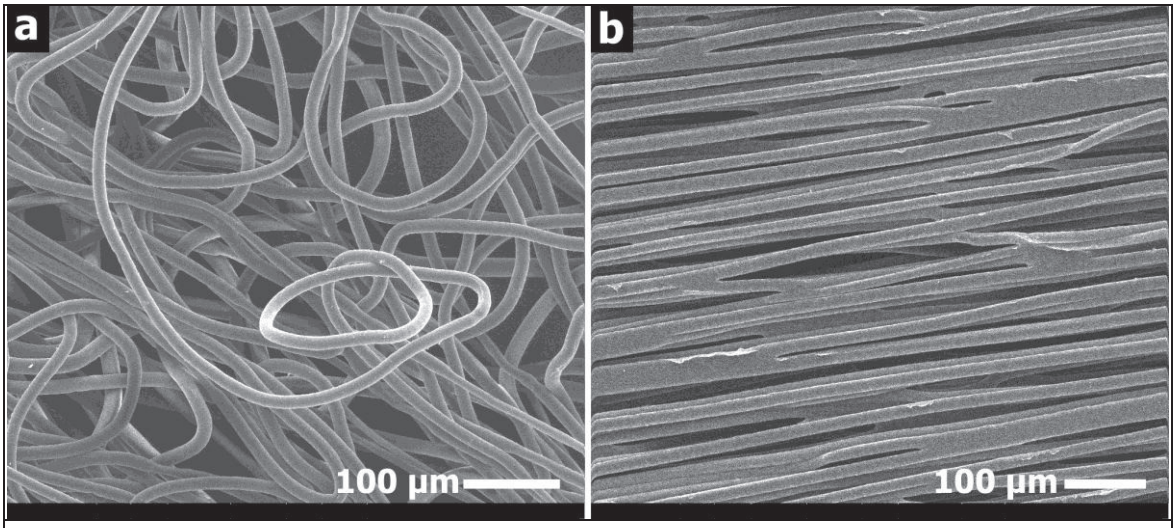

Figure 2 a & b

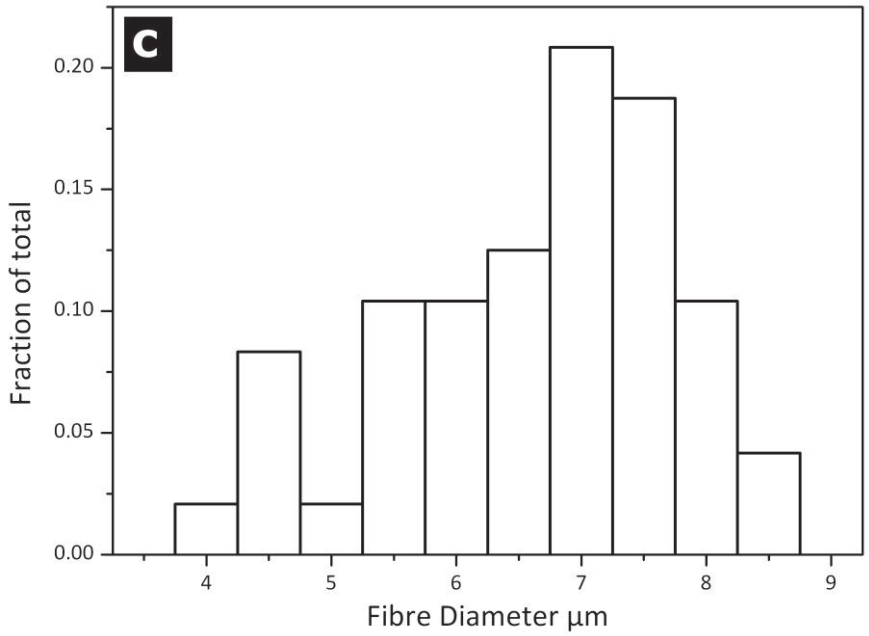

Figure 2c

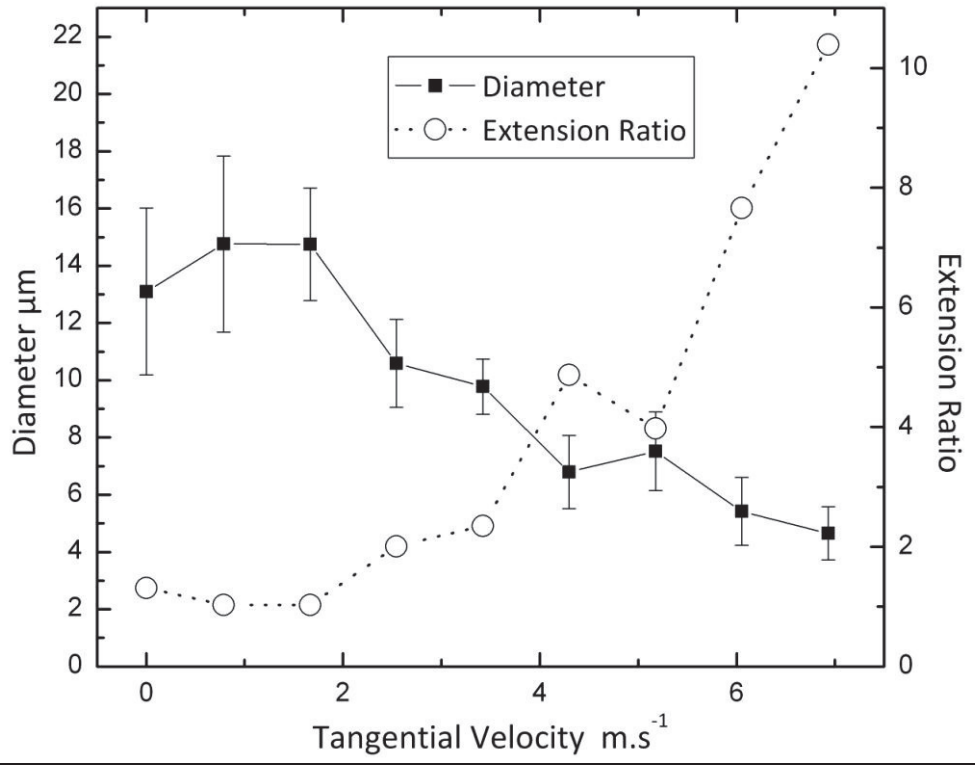

Figure 3

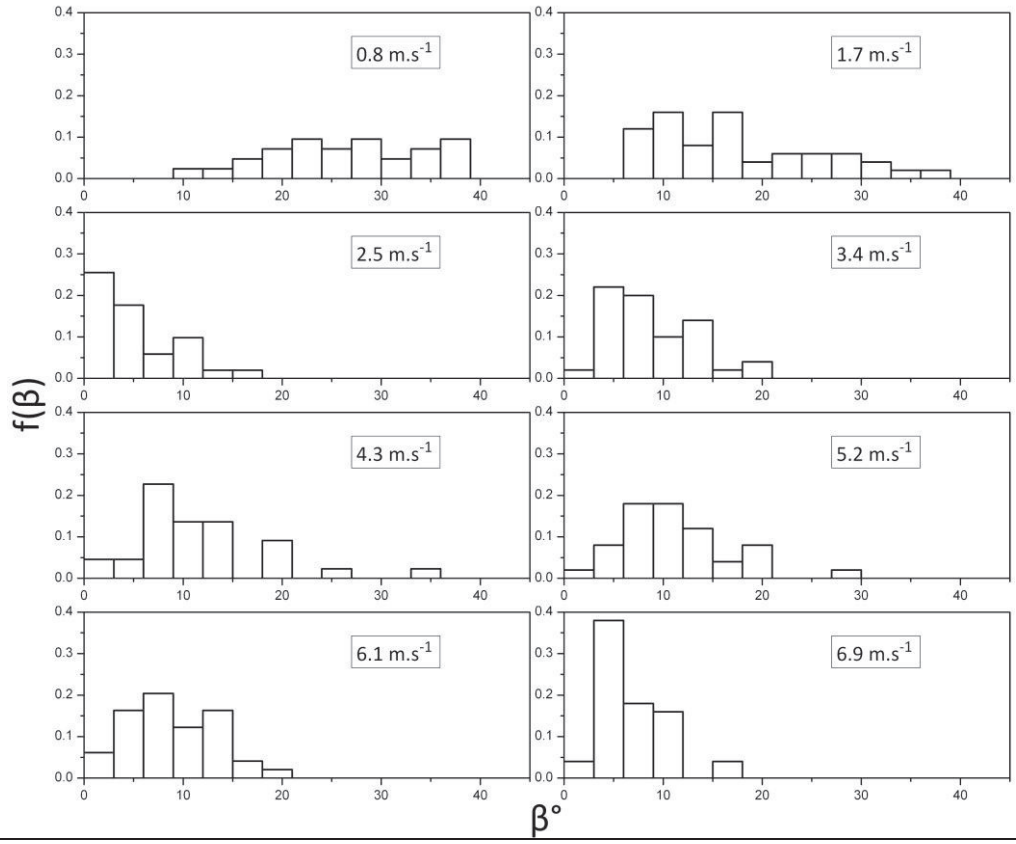

Figure 4

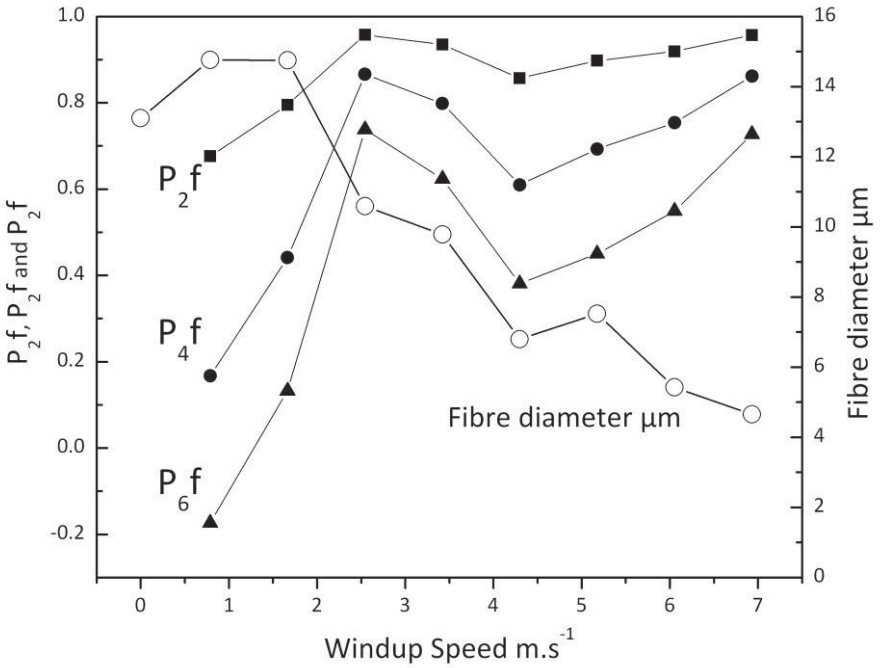

Figure 5

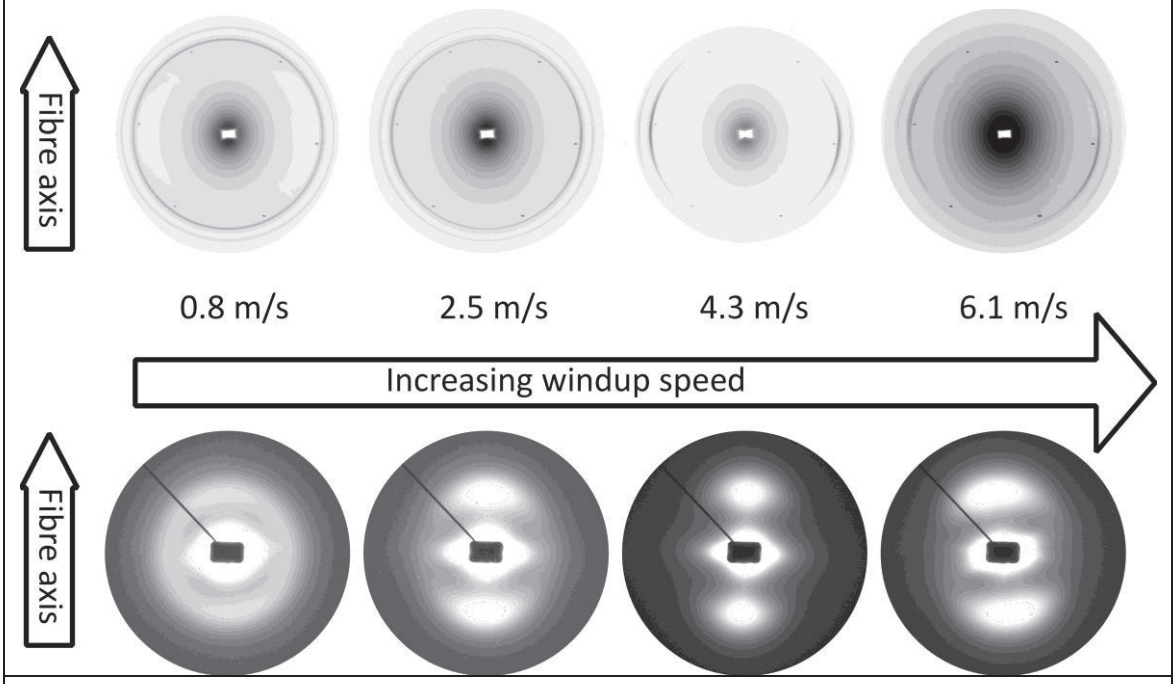

Figure 6

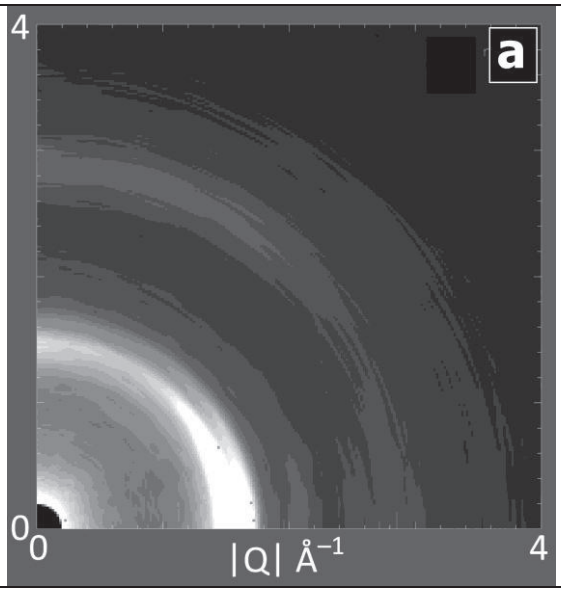

Figure 7a

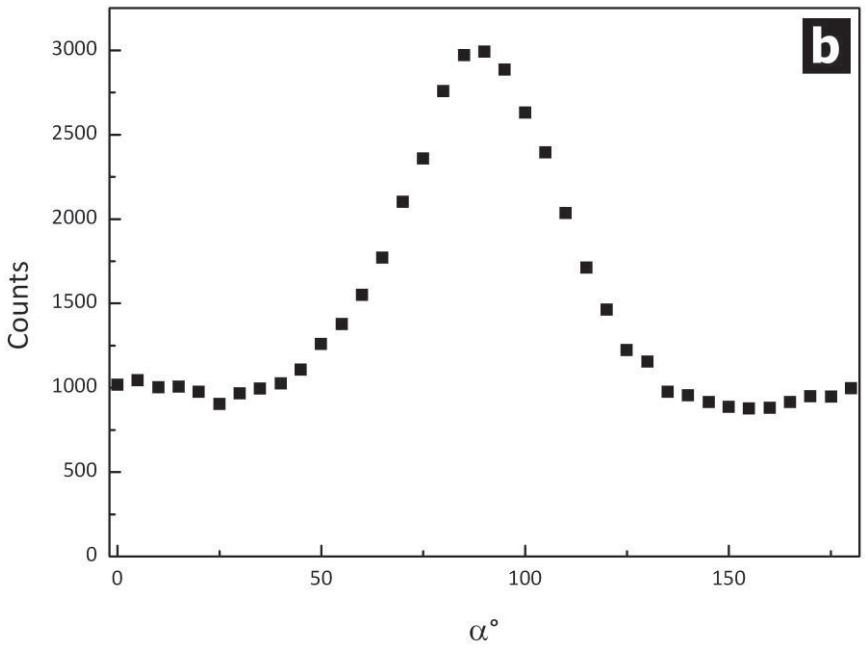

Figure 7b

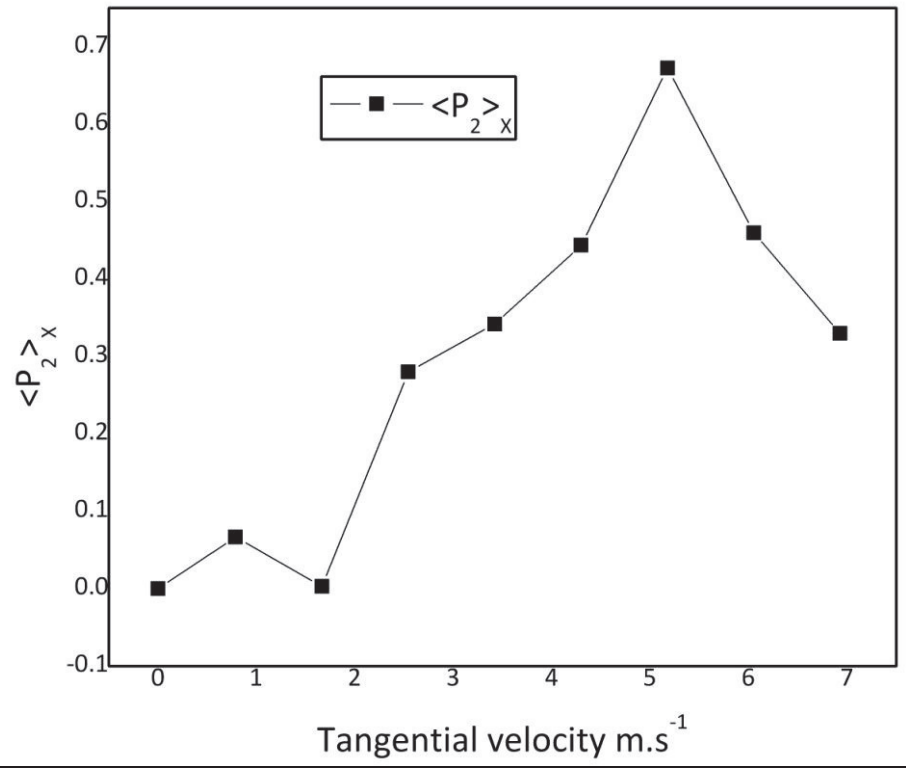

Figure 8

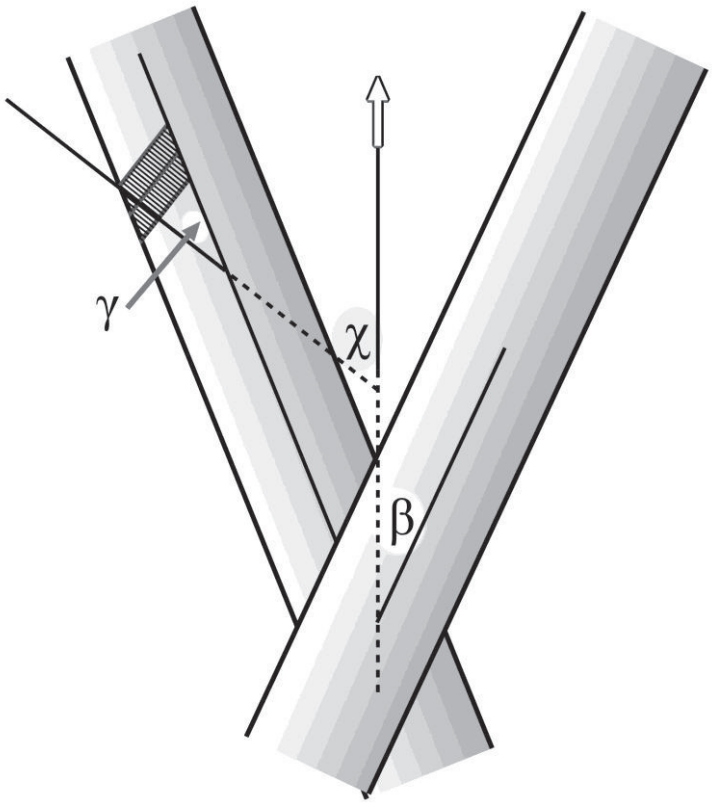

Figure 9

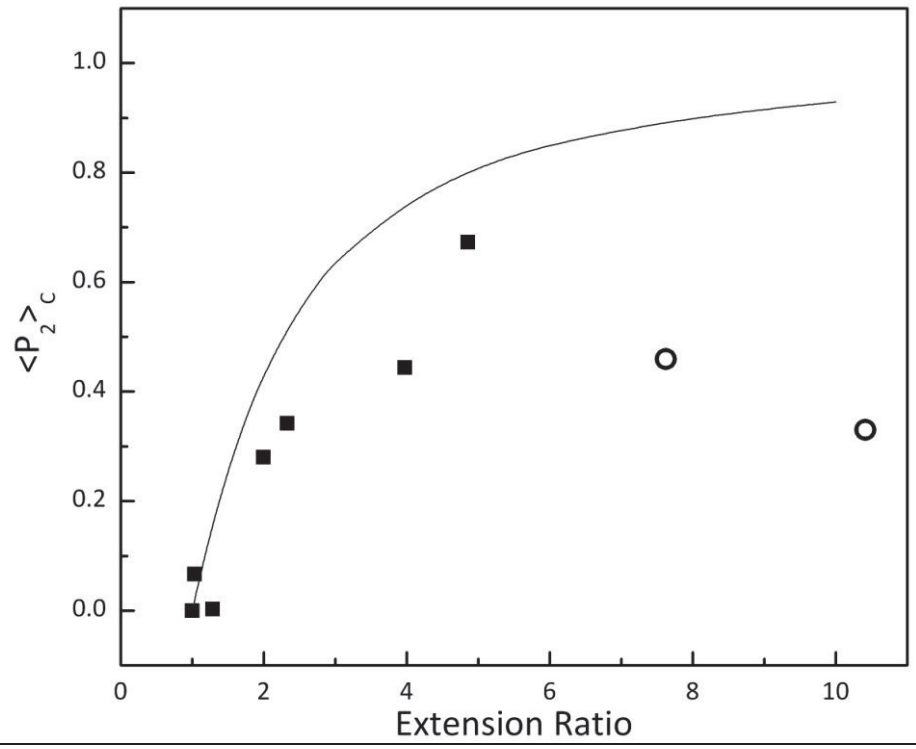

Figure 10